Synchronized photonic modulators driven by surface acoustic waves

A. Crespo-Poveda,[1] R. Hey,[2] K. Biermann,[2] A. Tahraoui,[2] P. V. Santos,[2] B. Gargallo,[3] P. Muñoz,[3,4] A. Cantarero,[1] and M. M. de Lima, Jr.[1,5]*

[1]*Materials Science Institute, Universitat de València, Valencia, Spain*
[2]*Paul Drude Institute for Solid State Electronics, Berlin, Germany*
[3]*iTEAM Research Institute, Universitat Politècnica de València, Valencia, Spain*
[4]*VLC Photonics S.L., Valencia, Spain*
[5]*Fundació General Universitat de València, Valencia, Spain*

**mmlimajr@uv.es*

Abstract: Photonic modulators are one of the most important elements of integrated photonics. We have designed, fabricated, and characterized a tunable photonic modulator consisting of two 180°-dephased output waveguide channels, driven by a surface acoustic wave in the GHz frequency range built on (Al,Ga)As. Odd multiples of the fundamental driven frequency are enabled by adjusting the applied acoustic power. A good agreement between theory and experimental results is achieved. The device can be used as a building block for more complex integrated functionalities and can be implemented in several material platforms.

OCIS codes: (230.1040) Acousto-optical devices; (230.3120) Integrated optics devices; (230.4110) Modulators.

References and links

1. S. Nakamura, Y. Ueno, and K. Tajima, "Femtosecond switching with semiconductor-optical-amplifier-based symmetric Mach-Zehnder-type all-optical switch," Appl. Phys. Lett. **78**, 3929–3931 (2001).
2. E. Camargo, H. Chong, and R. De La Rue, "2D photonic crystal thermo-optic switch based on AlGaAs/GaAs epitaxial structure," Opt. Express **12**, 588–592 (2004).
3. Y. Jiang, W. Jiang, L. Gu, X. Chen, and R. T. Chen, "80-micron interaction length Silicon photonic crystal waveguide modulator," Appl. Phys. Lett. **87**, 221105 (2005).
4. Y. A. Vlasov, M. O'Boyle, H. F. Hamann, and S. J. McNab, "Active control of slow light on a chip with photonic crystal waveguides," Nature **438**, 65–69 (2005).
5. B. Qi, P. Yu, Y. Li, Y. Hao, Q. Zhou, X. Jiang, and J. Yang, "Ultracompact electrooptic Silicon modulator with horizontal photonic crystal slotted slab," IEEE Photonic. Tech. L. **22**, 724–726 (2010).
6. M. M. de Lima, Jr. and P. V. Santos, "Modulation of photonic structures by surface acoustic waves," Rep. Prog. Phys. **68**, 1639–1701 (2005).
7. M. M. de Lima, Jr., M. Beck, R. Hey, and P. V. Santos, "Compact Mach-Zehnder acousto-optic modulator," Appl. Phys. Lett. **89**, 121104 (2006).
8. M. Beck, M. M. de Lima, Jr., E. Wiebicke, W. Seidel, R. Hey, and P. V. Santos, "Acousto-optical multiple interference switches," Appl. Phys. Lett. **91**, 061118 (2007).
9. M. Beck, M. M. de Lima, Jr., and P. V. Santos, "Acousto-optical multiple interference devices," J. Appl. Phys. **103**, 014505 (2008).
10. E. C. S. Barretto and J. M. Hvam, "Photonic integrated single-sideband modulator / frequency shifter based on surface acoustic waves," P. Soc. Photo-opt. Inst. **7719**, 771920 (2010).
11. J. F. Capmany, P. M. Muñoz, M. M. de Lima, Jr., and P. V. Santos, "Tuneable AWG device for multiplexing and demultiplexing signals and method for tuning said device," Patent Application WO 2012/152977 A1 (2012).

#193756 - $15.00 USD Received 11 Jul 2013; revised 15 Aug 2013; accepted 21 Aug 2013; published 6 Sep 2013

12. D. A. Fuhrmann, S. M. Thon, H. Kim, D. Bouwmeester, P. M. Petroff, A. Wixforth, and H. J. Krenner, "Dynamic modulation of photonic crystal nanocavities using gigahertz acoustic phonons," Nat. Photonics **5**, 605–609 (2011).
13. D. Yudistira, D. Janner, S. Benchabane, and V. Pruneri, "Integrated acousto-optic polarization converter in a ZX-cut $LiNbO_3$ waveguide superlattice," Opt. Lett. **34**, 3205–3207 (2009).
14. Q. J. Wang, C. Pflügl, W. F. Andress, D. Ham, F. Capasso, and M. Yamanishi, "Gigahertz surface acoustic wave generation on ZnO thin films deposited by radio frequency magnetron sputtering on III-V semiconductor substrates," J. Vac. Sci. Technol. B **26**, 1848–1851 (2008).
15. A. D. Barros, P. D. Batista, A. Tahraoui, J. A. Diniz, and P. V. Santos, "Ambipolar acoustic transport in silicon," J. Appl. Phys. **112**, 013714 (2012).
16. E. D. Palik, *Handbook of optical constants of solids* (Academic Press).
17. S. Adachi, "GaAs, AlAs, and $Al_xGa_{1-x}As$: material parameters for use in research and device applications," J. Appl. Phys. **58**, R1–R29 (1985).
18. M. M. de Lima, Jr., F. Alsina, W. Seidel, and P. V. Santos, "Focusing of surface-acoustic-wave fields on (100) GaAs surfaces," J. Appl. Phys. **94**, 7848–7855 (2003).

1. Introduction

Integrated photonics aims at controlling and manipulating photons within small dimensions. For that purpose, it is of paramount importance to search for devices that are at the same time fast, compact, efficient, low-cost, externally controlled, and compatible with nowadays integration technology. An interesting approach exploits non-linear optical effects for all-optical control. In this way, very fast devices are obtained with the drawback of very long interaction paths to compensate the usually very weak non-linearities [1]. Alternatively, thermo-optical effects allow the fabrication of smaller devices at the expense of longer time responses [2]. A further option employs electric fields in order to control the response of photonic devices by means of the electro-optic effect [3–5], leading to devices that are simultaneously fast and compact with the disadvantage of requiring the individual addressing of the regions to be tuned, which can become too difficult for complex architectures. A promising approach consists of using a surface acoustic wave (SAW) beam to modulate multiple ridge or slot waveguides (WGs) through the acousto-optical effect [6, 7]. This method presents an excellent compromise between speed and size and, even more important, allows the addressing of multiple devices using a single SAW due to its very large phase coherence [8–11]. Recently, SAWs have also been used to dynamically control planar nanocavities in photonic crystal membranes [12]. In addition, this technology can be employed in virtually any material platform with processing steps easily implemented in any modest cleanroom. For certain applications, the dynamic nature of the SAW requires the synchronization of the optical pulses with the SAW phase.

In this work, we have designed, fabricated, and characterized a tunable photonic modulator consisting of two 180°-dephased output WG channels driven by a SAW that can be used as a basic building block for more complex integrated photonic systems such as multiple WG modulators or tunable arrayed waveguide grating devices [11]. Although, we have implemented the concept in an (Al,Ga)As platform, it can be extended for other material platforms such as $LiNbO_3$ [13], (In,Ga)P [14], or Silicon [15].

2. Device concept

Figure 1 shows an overview of the structure we have exploited. The device follows a well-known regular Mach-Zehnder Interferometer (MZI) structure, built upon multimode interference (MMI) couplers. The first coupler is a balanced (50:50) splitting ratio MMI that separates the incoming light in identical beams delivered to two output ports. These WGs are modulated by a SAW beam propagating perpendicularly to them (MWG_1 and MWG_2, cf. Fig. 1). The MWGs feed a second MMI that combines the input light into 2 output waveguides (OWG_1 and OWG_2) with distribution power depending on the intensity and phase of the light leaving the

#193756 - $15.00 USD Received 11 Jul 2013; revised 15 Aug 2013; accepted 21 Aug 2013; published 6 Sep 2013

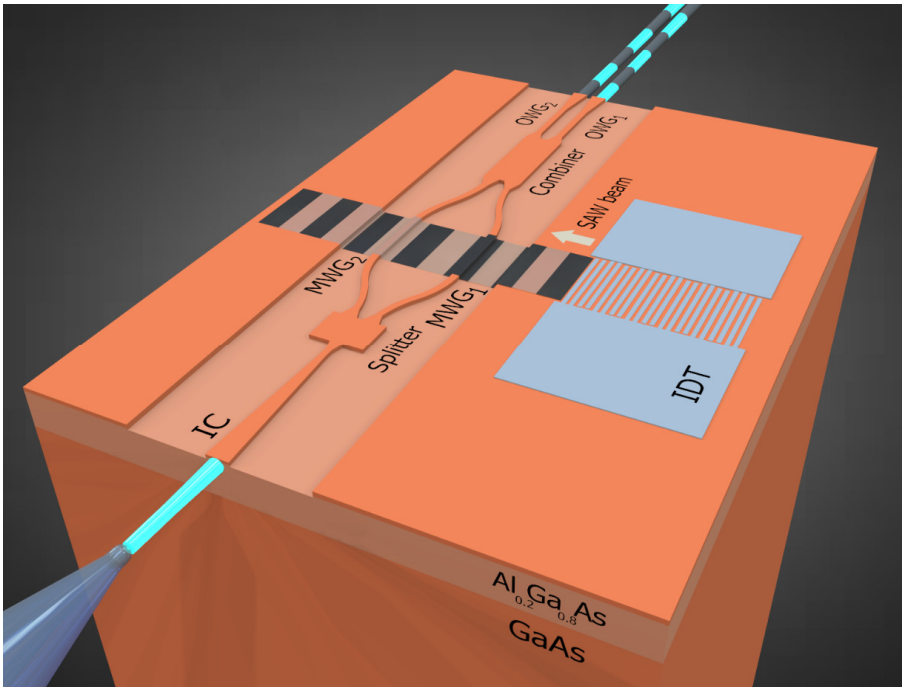

Fig. 1. Illustration (not to scale) of the SAW-driven synchronized modulator fabricated on (Al,Ga)As. By means of a tapered fiber, continuous light is coupled into an input channel (IC). The device consists of a splitter and a combiner MMI linked by waveguides (MGWs) that are modulated by a SAW generated by an IDT. The SAW propagates perpendicularly to the MGW arms. The light beams leaving the device through both output waveguides (OWGs) presents a 180°-dephasing synchronization. The spatial separation between the MWGs was chosen to be $1.5\lambda_{\mathrm{SAW}}$.

MWGs. The design of the combiner MMI is such that when both MWGs deliver light of equal intensity and phase, the intensity in the OWGs becomes also the same. This feature is granted in the absence of SAW by the splitter MMI. By introducing a phase difference between the MWGs ($\Delta\Phi = \delta\Phi_{\mathrm{MWG}_1} - \delta\Phi_{\mathrm{MWG}_2}$), the output power can be fully directed to OWG_1 (when $\Delta\Phi = +k\pi$, for $k = 1,2,3\ldots$) or to OWG_2 (when $\Delta\Phi = -k\pi$, for $k = 1,2,3\ldots$). $\Delta\Phi$ is obtained by the SAW modulation via the acousto-optical effect. A crucial aspect of the design is that the spatial separation between the WGs in the active region should be set to $(2m+1)\lambda_{\mathrm{SAW}}/2$, where λ_{SAW} is the surface acoustic wavelength, and m is an integer [7]. The MWGs are placed at the appropriate separation by means of large radius S-bend WGs. This ensures that each of the two MWGs suffers changes in the effective refractive index of equal magnitude but opposite phases, thus maximizing the overall acousto-optical effect. Therefore the magnitude of the phase difference introduced by the SAW for each one of the MWGs in the active region can be written according to:

$$|\delta\Phi_{\mathrm{MWG}_i}| = (2\pi\ell/\lambda_L)\delta n_{\mathrm{eff}} = a_P\sqrt{P_{\mathrm{IDT}}}, \tag{1}$$

with

$$n_{\mathrm{eff}} = n^0_{\mathrm{eff}} \pm \delta n_{\mathrm{eff}}\cos(\omega_{\mathrm{SAW}}t). \tag{2}$$

Here, ℓ is the length of the MWG, λ_L is the light wavelength, a_P is a proportionality constant

#193756 - $15.00 USD Received 11 Jul 2013; revised 15 Aug 2013; accepted 21 Aug 2013; published 6 Sep 2013

that depends on the materials elasto-optical properties as well as on the overlap between the optical and acoustic fields in the MWG. P_{IDT} is the nominal radio-frequency (RF) power applied to the interdigital transducer (IDT), n^0_{eff} is the unperturbed effective refractive index, δn_{eff} is the amplitude of the SAW modulation in the effective refractive index, and ω_{SAW} is the SAW angular frequency. Finally, the signal is positive for $i = 1$ and negative for $i = 2$. In contrast to previously realized modulators [7–9] where part of the light transmission is lost due to destructive interference, in our approach, at any given time, the light only switches paths, avoiding losses and granting the 180°-dephasing synchronization of the OWGs.

3. Design and simulation

In order to optimize the response of the devices, we have simulated their performance using the beam propagation method implemented via the RSoft package. The operational optical wavelength was chosen to be of approximately 900 nm, which falls within our fast detector sensitivity range. The refractive indices used for the simulations were $n^{900}_{\mathrm{GaAs}} = 3.591$ [16] and $n^{900}_{\mathrm{Al_{0.2}Ga_{0.8}As}} = 3.421$ [17]. Assuming either the transverse electric (TE) or the transverse magnetic (TM) optical polarizations at the input waveguide, we tracked the intensity of the optical field throughout the device. The effects of the SAW modulation is included by modifying the effective refractive index of the MWGs according to Eq. (2). Figure 2 shows the results of the simulations for $\delta n_{\mathrm{eff}} = 0.0011$ and TE propagation for three different times ($t = 0,\ T_{\mathrm{SAW}}/4 \approx 480$ ps, and $T_{\mathrm{SAW}}/2 \approx 960$ ps). For $t = 0$ (upper panel) all light goes to OWG_1 while for $t = T_{\mathrm{SAW}}/2$ (bottom panel) all the optical power is delivered to OWG_2. When $t = T_{\mathrm{SAW}}/4$ (central panel) the cosine term in Eq. (2) vanishes and the device operates as in the absence of a SAW, with the optical power equally distributed between both OWGs.

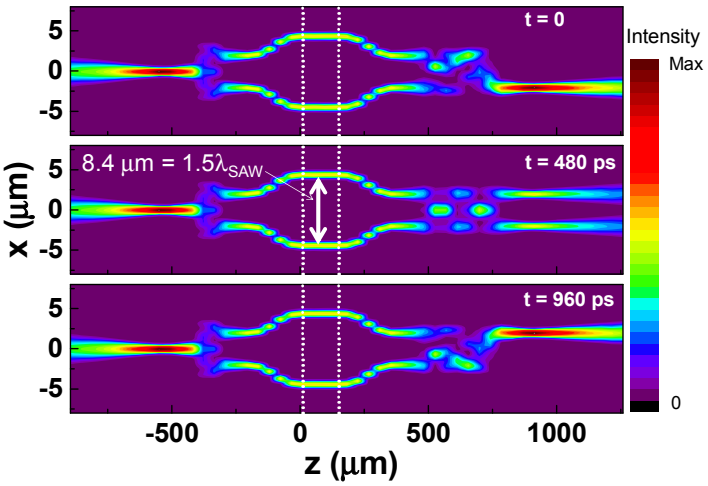

Fig. 2. Color map of the optical intensity as the light propagates through the device for different times calculated assuming $\delta n_{\mathrm{eff}} = 0.0011$. The area between the vertical dotted lines corresponds to the active region modulated by the SAW beam in which the waveguides are separated by $1.5\lambda_{\mathrm{SAW}}$.

4. Sample and device fabrication

The device was fabricated on a sample grown by molecular beam epitaxy on a (100) GaAs substrate. The sample consists of a 1500-nm-thick $\mathrm{Al_{0.2}Ga_{0.8}As}$ cladding layer capped by a

#193756 - $15.00 USD Received 11 Jul 2013; revised 15 Aug 2013; accepted 21 Aug 2013; published 6 Sep 2013

300-nm-thick GaAs guiding layer. The modulators were fabricated in two steps using contact optical lithography. First, Ti/Al/Ti IDTs in a split-finger configuration for efficient SAW generation were fabricated using a lift-off process [18]. These IDTs were designed for $\lambda_{SAW} = 5.6\ \mu$m (with finger width and spacing of 700 nm), which corresponds to a resonance frequency of approximately 520 MHz. A second step of plasma etching was then employed to create 465-nm-deep grooves delimiting the ridge WGs. The length of the MWGs in the active region is $\ell = 120\ \mu$m, as determined by the IDT aperture. The MWGs width was chosen to be 900 nm, which is much smaller than λ_{SAW}, ensuring a constant amplitude modulation through the WG width while allowing for reliable fabrication using contact optical lithography and etching techniques. The separation between the center of the MWGs was set to be $1.5\lambda_{SAW}$. The width and length of the splitter MMI are 7 μm and 110 μm, respectively, while for the combiner MMI, the width is 6 μm and the length is 314 μm. Details of the fabricated devices can be seen in the photographs shown in Figs. 3(a)–3(c).

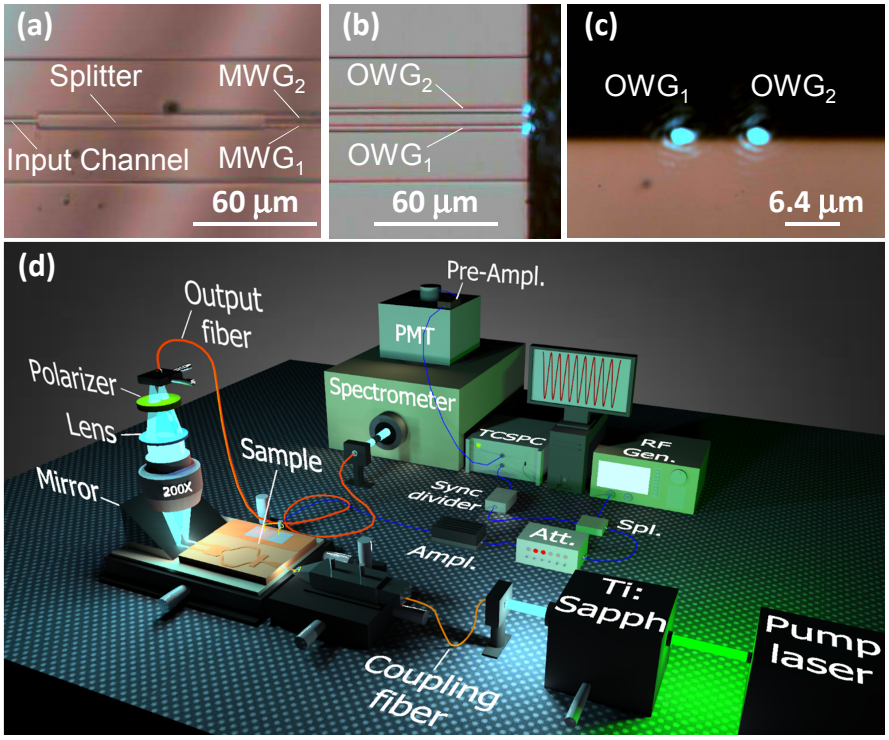

Fig. 3. Top view photograph of the splitter MMI (a), as well as, top (b) and lateral (c) view of the OWGs. In (b) and (c) false color, time-integrated image of the infra-red light leaving both OWGs can also be observed. (d) Artistic illustration (not to scale) of the experimental setup used to measure the time response of the light transmission through the device. A 200× objective with focal plane located at the edge of the sample collects the light from the OWGs. A polarizer is used to filter the TE or the TM modes. A multi-mode fiber placed at the image plane selects the light from one of the OWGs for detection by a photomultiplier tube (PMT) synchronized with the RF signal that generates the SAWs. In order to obtain synchronization (sync.), the signal from the RF generator (RF gen.) is sent to a splitter (spl.) in a way that 50% of the signal has its frequency divided by 10. This is necessary to keep the trigger within the operational frequency range of the time-correlated single photon counting (TCSPC) module. The other half of the signal goes through a controllable attenuator (att.), a fixed-gain amplifier (ampl.) and then drives the interdigital transducer.

#193756 - $15.00 USD Received 11 Jul 2013; revised 15 Aug 2013; accepted 21 Aug 2013; published 6 Sep 2013

5. Experimental setup

The device was optically characterized by coupling light into the input WG using a tapered fiber whose tip has the form of a cylindrical lens (Fig. 1). An overview of the experimental setup is illustrated in Fig. 3(d). As light source, we used a tunable Ti:Sapphire laser operating at ≈ 0.9 μm pumped by a 532 nm diode laser. The fiber was mounted on a X-Y-Z stage, allowing for an accurate positioning relative to the input WG edge. The transmitted light was reflected by a right angle mirror facing the edge of the OWGs. The light was then collected by a long working distance 200$\times$ Mitutoyo microscope objective focused on the device edge [cf. Fig. 3(c)] and coupled to an optical fiber. The large objective magnification allows for the spatial selection of the individual OWG to be measured. The propagation of TE or TM modes was filtered by a linear polarizer placed before the coupling to the output fiber. As detector, a micro-channel plate photomultiplier tube (PMT) with a time resolution of 300 ps was employed. In order to grant synchronization with the detector, the RF-signal from the generator was first split. One half passed through a controllable attenuator, a fixed gain amplifier and was then used to drive the IDT. The second half was first divided by 10 (in order to be within the frequency range of the electronics of the detector controller) and then used to trigger the detector.

6. Results

Figure 4 shows results obtained for transmission through both OWGs of light with TE polarization (similar behavior was observed for TM polarization) for different P_{IDT}. The total transmission is normalized to 1. At small P_{IDT} values [Fig. 4(a)] a very weak modulation is observed with both OWGs transmitting near 50% of the total light. As P_{IDT} raises, the modulation becomes stronger, reaching a peak-to-peak amplitude of approximately 1 in our experiments, for $P_{\mathrm{IDT}} = 14$ μW [see Fig. 4(b)]. After the modulation reaches its maximum, the appearance of higher harmonics becomes evident [Fig. 4(c)]. For $P_{\mathrm{IDT}} = 96$ μW the light modulation is dominated by the third harmonic [Fig. 4(d)]. This can be better appreciated by performing a fast Fourier transform (FFT) analysis of the obtained experimental results. Figure 5 shows the FFT coefficients for the first three harmonics ($h1, h2,$ and $h3$, respectively) of the time resolved experimental data (as a function of $\sqrt{P_{\mathrm{IDT}}}$, upper scale) as well as for the simulations (as a function of δn_{eff}, lower scale). The phase difference between the OWGs was found experimentally to be

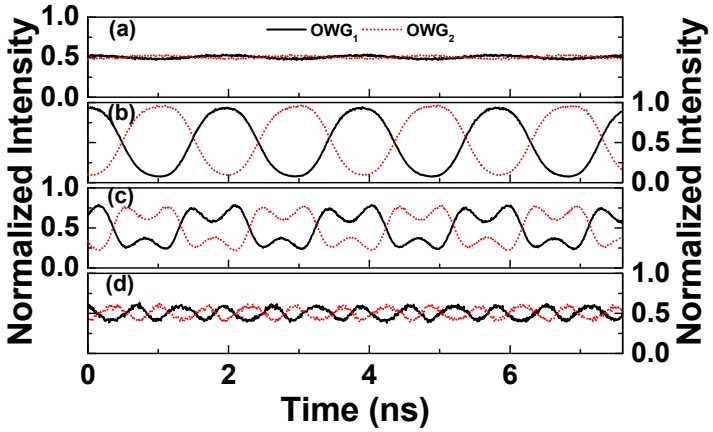

Fig. 4. Time-resolved measurements of the light leaving the OWG_1 (solid line) and OWG_2 (dotted line) for RF powers of (a) $P_{\mathrm{IDT}} = 15$ nW, (b) $P_{\mathrm{IDT}} = 14$ μW, (c) $P_{\mathrm{IDT}} = 70$ μW and (d) $P_{\mathrm{IDT}} = 96$ μW measured for the TE polarization.

#193756 - $15.00 USD Received 11 Jul 2013; revised 15 Aug 2013; accepted 21 Aug 2013; published 6 Sep 2013

$180^\circ \pm 3^\circ$. By comparing both data with Eq. (1), we determined that $a_P \approx 13 \times 10^{-2}$ rad$/\sqrt{mW}$, which is a factor of 2 larger than that obtained in Ref. [7] for a single, SAW-modulated, Mach-Zehnder interferometer. In general, there is a very good agreement between the measurements on the fabricated device and the simulations for the idealized case. It is clear from Fig. 5 that both the $h1$ and $h3$ intensities, although slightly smaller than that predicted, follow almost perfectly the calculated trend. Furthermore, the vanishing of $h1$ close to $\delta n_{\text{eff}} = 3 \times 10^{-3}$ is very well reproduced by the simulations. The presence in our experiments of a larger $h2$ than expected is attributed to asymmetric imperfections in the fabrication process. In addition, the values obtained in the measurements of $h3$, which has an oscillation period of ≈ 600 ps, are substantially limited by the time resolution of 300 ps. This explains the reduced values for the FFT coefficients for $h3$ shown in Fig. 5 as well as the low amplitude of the time response trace of Fig. 4(d).

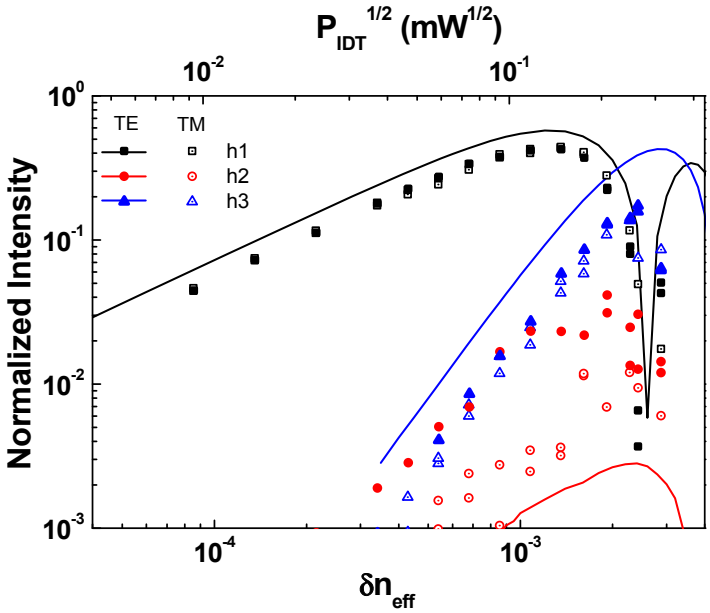

Fig. 5. Experimental (symbols) values for the fast Fourier transform coefficients of the time-resolved signals for the first, second and third harmonics ($h1 = 517$ MHz, $h2 = 1.03$ GHz, and $h3 = 1.55$ GHz, respectively) as a function of the square root of P_{IDT} (upper scale). Simulated results for the TE modes (lines), as a function of δn_{eff} (lower scale), are also shown. The full and open symbols correspond to TE and TM modes, respectively.

7. Conclusion

In conclusion, we have realized a SAW-driven photonic modulator based on a MZI that operates in the GHz frequency range. The device delivers the continuous-wave input light to two, 180°-dephased, synchronized output ports, whose frequency and amplitude response can be tuned by varying the acoustic power. In particular, the operational frequency of the device can be adjusted to be an odd multiple of the fundamental frequency driving the SAWs. Another advantage of our approach is that the very large phase coherence of the SAWs allows for the control of multiple devices with the same SAW, a feature that is beneficial for integration in more complex architectures.

#193756 - $15.00 USD Received 11 Jul 2013; revised 15 Aug 2013; accepted 21 Aug 2013; published 6 Sep 2013

Acknowledgments

We thank J. Pedrós for helping with the sample preparation. This work has been supported by the international campus of excellence VLC/CAMPUS and by the program INNCIDE from the Spanish Ministry of Economy and Competitiveness (MINECO), through the program "*Valoritza i Transfereix*" from the Vice-Principal of Research and Scientific Policy of the Universitat de València and through the program INNOVA (grant SP20120860) from the Universitat Politècnica de València. The authors also acknowledge financial support by the Spanish MINECO Projects TEC2010-21337 and MAT2012-33483. A. Crespo-Poveda and B. Gargallo acknowledge financial support through FPI grants BES-2010-036846 and BES-2011-046100, respectively.

#193756 - $15.00 USD Received 11 Jul 2013; revised 15 Aug 2013; accepted 21 Aug 2013; published 6 Sep 2013